Extended filamentation with temporally chirped femtosecond Bessel-Gauss beams in air

Pavel Polynkin[1], **Miroslav Kolesik**[1,2], **Jerome Moloney**[1,2]

[1] *College of Optical Sciences, The University of Arizona, Tucson, Arizona 85721, USA*
[2] *Department of Mathematics, The University of Arizona, Tucson, Arizona 86721, USA*

ppolynkin@optics.arizona.edu

Abstract: We report experimental results on ultrafast filamentation with temporally chirped femtosecond Bessel-Gauss beams. We find that by chirping the pulses, the longitudinal range of the generated plasma channels can be extended relative to filaments generated by fully compressed, transform-limited femtosecond pulses. We find a clear correlation between the extent of filamentation and the intensity of the on-axis emission by the femtosecond Bessel-Gauss beam. The on-axis emission is negligible for fully compressed pulses, but it can become quite substantial (up to 10% of the input pulse energy) when chirped pulses are used. Under certain conditions, the on-axis emission becomes sufficient for generating its own plasma channel thus resulting in extended filamentation. This effect may offer means of remote control over filament formation with femtosecond Bessel-Gauss beams. We identify a four-wave mixing process, enhancement of which is likely to result in a maximum of the on-axis emission, and derive a simple expression for estimating the duration of the chirped pulse that is required for such enhancement. Our estimations are in good agreement with the experiment.

OCIS codes: (320.2250) Femtosecond phenomena; (320.7110) Ultrafast nonlinear optics; (350.5400) Plasmas

References and links

1. A. Couairon and A. Mysyrowicz, "Femtosecond filamentation in transparent media," Phys. Rep. **441**, 47–189 (2007).
2. A. Ishaaya, L. Yuong, T. Grow, and A. Gaeta, "Self-focusing dynamics of polarization vortices in Kerr media," Opt. Lett. **33**, 13–15 (2008).
3. M. Chateauneuf, S. Payeur, J. Dubois, and J.-C. Kieffer, "Microwave guiding in air by a cylindrical filament array waveguide," Appl. Phys. Lett. **92**, 091104 (2008).
4. J. Durnin, J. Miceli, and J. Eberly, "Diffraction-free Beams," Phys. Rev. Lett. **58**, 1499–1501 (1987).
5. J. Lit and R. Tremblay, "Focal depth of a transmitting axicon," J. Opt. Soc. Am. **63**, 445–449 (1973).
6. Q. Luo, H. Xu, S. Husseini, J.-F. Daigle, F. Théberge, M. Sharifi, and S. Chin, "Remote sensing of pollutants using femtosecond laser pulse fluorescence spectroscopy," Appl. Phys. B **82**, 105–109 (2006).
7. J. Kasparian, R. Ackermann, Y. André, G. Méchain, G. Méjean, B. Prade, P. Rohwetter, E. Salmon, K. Stelmaszczyk, J. Yu, A. Mysyrowicz, R. Sauerbrey, L. Wöste, and J. Wolf, "Electric events synchronized with laser filaments in thunderclouds," Opt. Express **16**, 5757–5763 (2008).
8. I. Golub, "Superluminal-source-induced emission," Opt. Lett. **20**, 1847–1849 (1995).

#103538 - $15.00 USD Received 3 Nov 2008; revised 29 Dec 2008; accepted 3 Jan 2009; published 7 Jan 2009

9. S. Klewitz, S. Sogomonian, M. Woerner, and S. Herminghaus, "Stimulated Raman scattering of femtosecond Bessel beams," Opt. Commun. **154**, 186–190 (1998).
10. R. Gadonas, V. Jarutis, R. Paškauskas, V. Smilgevicius, A. Stabinis, and V. Vaičaitis, "Self-action of Bessel beam in nonlinear medium," Opt. Commun. **196**, 309–316 (2001).
11. C. Durfee III, and H. Milchberg, "Light pipe for high intensity laser pulses," Phys. Rev. Lett. **71**, 2409–2412 (1993).
12. A. York, B. Layer, J. Palastro, T. Antonsen, and H. Milchberg, "Ultrahigh-intensity optical slow-wave structure for direct laser electron acceleration," J. Opt. Soc. Am. B **25**, B137-B146 (2008).
13. C.-H. Pai, M.-W. Lin, L.-C. Ha, S.-T. Huang, Y.-C. Tsou, H.-H. Chu, J.-Y. Lin, J. Wang, and S.-Y. Chen, "Backward Raman amplification in a plasma waveguide," Phys. Rev. Lett. **101**, 065005 (2008).
14. P. Polynkin, M. Kolesik, A. Roberts, D. Faccio, P. Di Trapani, and J. Moloney, "Generation of extended plasma channels in air using femtosecond Bessel beams," Opt. Express **16**, 15733–15740 (2008).
15. S. Akturk, B. Zhou, M. Franco, A. Couairon, and A. Mysyrowicz, "Generation of long plasma channels in air by focusing ultrashort laser pulses with an axicon," Opt. Commun. **282**, 129–134 (2009).
16. S. Tewari, H. Huang, and R. Boyd, "Theory of self-phase matching," Phys. Rev. A **51**, R2707–R2710 (1995).
17. A. Dubietis, P. Polesana, G. Valiulis, A. Stabinis, P. Di Trapani, and A. Piskarkas, "Axial emission and spectral broadening in self-focusing of femtosecond Bessel beams," Opt. Express **15**, 4168–4175 (2007).
18. M. Mlejnek, E. Wright, and J. Moloney, "Dynamic spatial replenishment of femtosecond pulses propagating in air," Opt. Lett. **23**, 382–384 (1998).
19. A. Friberg, "Stationary-phase analysis of generalized axicons," J. Opt. Soc. Am. A **13**, 743–750 (1996).

1. Introduction

Ultrafast filamentation in dielectrics is a rich and interdisciplinary science that crosses boundaries between plasma physics, nonlinear optics and material science. Most of the early studies, both experimental and theoretical, involved generation of plasma channels using femtosecond laser pulses with Gaussian or flat-top transverse beam profiles (for a recent review see [1]). As this field matured, filamentation studies moved on to exploring more complex beam profiles such as vortex beams [2], ring-shaped beams [3] and Bessel-like beams.

Bessel beams have been known in linear optics for over twenty years [4]. In a linear medium, these beams represent a particular solution of the wave equation that remains invariant on propagation. An ideal Bessel beam that is truly diffraction-free has infinite energy and thus cannot be realized experimentally. However, truncated or apodized Bessel beams, that can be realized, retain certain diffraction-free properties. Perhaps the most practically relevant Bessel-like beam with finite energy is the Bessel-Gauss beam that can be generated by passing a collimated Gaussian beam through a conical lens called axicon [5]. Extended linear foci of Bessel-Gauss beams make them particularly suited for studies in ultrafast laser filamentation. Long and stable plasma channels generated by such beams are of interest in various potential applications such as remote spectroscopy [6] and atmospheric science [7].

Filamentation and ultrafast nonlinear optics with Bessel-like beams were extensively studied in condensed media such as fused silica, water and benzene [8]-[10]. In gaseous media, ultraintense Bessel-like beams were used for generating few centimeter-long plasma waveguides [11] for use in particle acceleration [12] and backward Raman amplification [13]. Recently, experiments on generation of extended plasma channels in air using femtosecond Bessel-Gauss beams have been reported [14],[15]. An interesting effect reported in [14] was the observed longitudinal extension of the generated plasma channels resulting from temporally chirping laser pulses. It was found that while fully compressed femtosecond pulses created plasma channels that covered the entire extent of the linear focus zone of the Bessel-Gauss beam, a particular value of temporal pulse chirp resulted in filamentation extending beyond the linear focus zone. The longitudinal extension of filamentation was found to occur for both positive and negative values of the pulse chirp.

Extending the longitudinal range of filamentation by pulse chirping is a practically important effect as it can offer means of control over filament formation. The physical mechanisms responsible for this effect have not been clarified. In this paper we report experiments that es-

#103538 - $15.00 USD Received 3 Nov 2008; revised 29 Dec 2008; accepted 3 Jan 2009; published 7 Jan 2009

tablish a correlation between the longitudinal extension of filaments and the magnitude of the on-axis emission by the chirped Bessel-Gauss beams. We find that the fraction of the pulse energy that is re-emitted along the beam axis can exceed 10% of the input pulse energy for a particular value of the temporal pulse chirp. The same chirp value also results in the longest generated plasma channel. Thus, under particular conditions, the on-axis intensity emitted by the beam becomes high enough to generate a plasma channel on its own. The resulting secondary plasma channel is connected to that generated by the primary Bessel-Gauss beam, and this is the mechanism responsible for filament extension by chirping.

Studies of the nonlinear transverse reshaping of Bessel-like beams on propagation in nonlinear media typically involve numerical evaluation of the transverse phase-matching integral [16]. Using this approach, self-action of a *quasi-CW* Bessel-Gauss beam in a nonlinear medium was studied, and the participating nonlinear processes were identified [10]. Similar approach was recently used in [17] to analyze axial emission by *femtosecond* Bessel-like beams in water. To analyze our results, we identify the dominant nonlinear-conversion process, enhancement of which is likely to result in the maximum on-axis emission by the beam. Based on plasma-assisted phasematching considerations, we derive a simple formula for the duration of the chirped pulse that results in the enhancement of the on-axis emission. Results of our analysis are in good agreement with the experiments.

2. Experimental setup

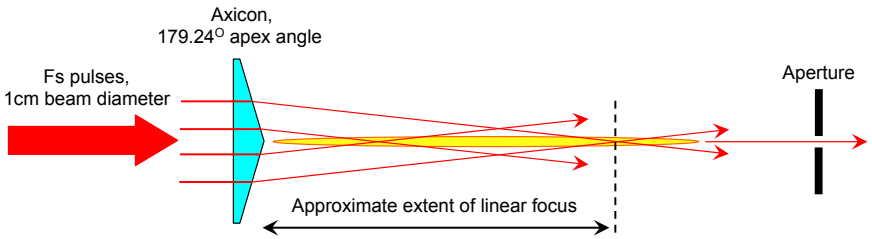

Fig. 1. Experimental setup. The aperture placed 4 m away from the axicon is used to isolate light propagating along the beam axis in the far-field.

The experimental setup is shown schematically in Fig. 1. The ultrafast laser source that we use in the experiments is a commercial Chirped-Pulse Amplification (CPA) Ti:Sapphire system that generates pulses at a repetition rate of 10 Hz. The maximum pulse energy attainable from the system is 35 mJ, at 800 nm center wavelength. Using a pulse shaper between the seed oscillator and the amplifier chain, we compensate for the nonlinear pulse distortions in the amplifiers. As a result, the system generates clean transform-limited pulses with a Gaussian temporal envelope. The temporal FWHM width of the fully compressed pulses is 35 fs as measured by a single-shot intensity autocorrelator.

The output of the laser has a clean Gaussian transverse profile with a 10 mm beam diameter and a beam-quality factor (M^2) specified by the manufacturer at 1.5. To generate a Bessel-Gauss beam, the laser is focused with an uncoated fused-silica axicon lens. The full apex angle of the axicon is 179.24°. At the maximum pulse energy of 35 mJ, multiple closely packed filaments are formed on the axis of the beam. To operate in the single-filament regime, we limit the pulse energy incident on the axicon to 15 mJ, by reflecting the laser beam off a coated beamsplitter plate. The beamsplitter that we use has a 22 mm-wide round clear aperture, and it weakly apertures the input Gaussian beam incident on the axicon. The resulting aperture size is 22mm in the vertical dimension, and $22\text{mm}/\sqrt{2} \approx 15.6\text{mm}$ in the horizontal dimension. The

#103538 - $15.00 USD Received 3 Nov 2008; revised 29 Dec 2008; accepted 3 Jan 2009; published 7 Jan 2009

maximum energy of the pulses, after passing through the uncoated axicon, is about 14 mJ.

The axicon lens that we use is 2 mm thick. To quantify the extent to which the axicon glass affects the spectral and temporal profiles of the laser pulses, we substituted the axicon with a 2mm-thick fused silica plate and characterized the pulses after passing through the plate. We found that, at the maximum pulse energy used in the filamentation experiments (14 mJ after the axicon), the pulse spectrum broadened in the glass plate by $\sim$20% but remained smooth. The temporal broadening of the 35 fs pulses in the glass was not measurable.

The pulse compressor in our CPA system incorporates a folding mirror on a motorized stage which allows for the total optical pathlength in the compressor to be remotely controlled. Using the single-shot intensity autocorrelator, we calibrated the compressor stage by recording the dependence of the FWHM duration of the pulses on the travel of the stage.

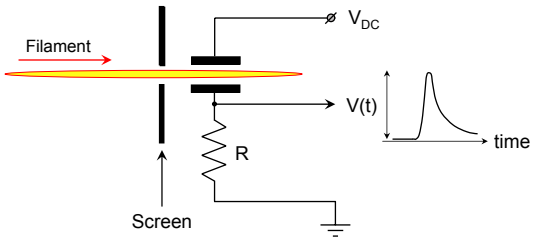

Fig. 2. Setup for probing local charge density in the plasma channel.

The plasma density along the filament is measured using a simple setup that is schematically shown in Fig. 2. The detailed description of this system can be found in [14]. In the experiments reported here, the electrodes are round and 7 mm in diameter. The distance between the electrodes is 1.5 mm, and the applied DC voltage is 1 kV.

In order to measure the pulse energy propagating on the beam axis in the far field, we use an aperture that is located at a distance of 4 m from the axicon and an energy meter placed immediately behind the aperture. The aperture diameter can be varied, which allows us to study the radial intensity distribution in the far-field.

3. Experimental results

Using the setup shown in Fig. 2, we measured the linear plasma density along the filamentation path for different values of the FWHM pulselength of the chirped laser pulses. We studied both positive and negative pulse chirps that were introduced by under- and over-compressing the pulses generated by the CPA laser system. The pulse energy was fixed at 14 mJ. We found that as the pulse duration increased, the length of the generated plasma channels was first steadily growing, then reached a maximum and started to decrease. This trend was observed for both positive and negative values of the pulse chirp, although positively chirped pulses generated somewhat longer plasma channels than negatively chirped pulses with the same FWHM pulselength.

The experimental data for the linear plasma density along the filament is shown in Fig. 3 (top), for cases of the shortest pulse used in the experiments (35 fs duration) and for the chirped pulses that generated longest filaments. These pulse durations were found to equal 660 fs (positively chirped pulses, long wavelengths travel ahead of short wavelengths) and 615 fs (negatively chirped pulses). In the bottom of Fig. 3 we show the on-axis intensity along the beam axis in the linear propagation regime. This data was taken with a strongly attenuated beam, using a fast photodetector with a 100μm pinhole in front of the detector.

In order to pinpoint the origin of the extended filamentation with chirped pulses, we measured

#103538 - $15.00 USD Received 3 Nov 2008; revised 29 Dec 2008; accepted 3 Jan 2009; published 7 Jan 2009

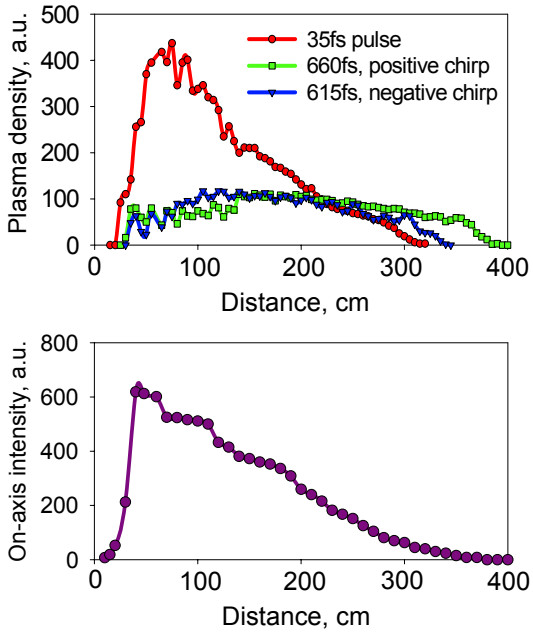

Fig. 3. Top: Linear plasma density along the filament for the fully compressed pulse and for positively and negatively chirped pulses that maximize the longitudinal extent of the plasma channel. Pulse energy is 14 mJ in all cases. Bottom: On-axis intensity of the Bessel-Gauss beam in the linear propagation regime.

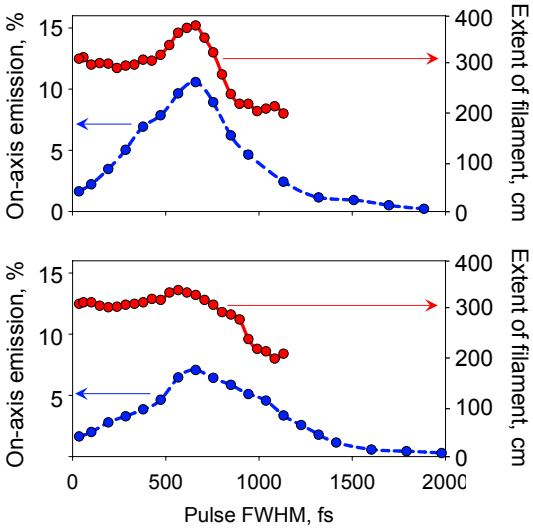

Fig. 4. Longitudinal range of the plasma channel and the fraction of the input pulse energy re-emitted by the beam along the beam axis, as functions of the FWHM pulselength. Top figure: Positively chirped pulses. Bottom figure: Negatively chirped pulses. The maximum fraction of the on-axis energy is over 10% and 7% for positively and negatively chirped pulses, respectively.

#103538 - $15.00 USD Received 3 Nov 2008; revised 29 Dec 2008; accepted 3 Jan 2009; published 7 Jan 2009

the on-axis intensity propagating close to the beam axis in the far field, as a function of the FWHM pulselength. For these measurements, the diameter of the aperture shown in Fig. 1 was set at 3 mm. The results of the measurements are summarized in Fig. 4, for positively chirped pulses (top) and negatively chirped pulses (bottom). The magnitude of the on-axis emission is shown in % relative to the input energy of the laser pulses. In the same plots, we show the longitudinal extent of the generated plasma channels. In these plots, the extent of filamentation is defined as the longitudinal coordinate at which the generated plasma becomes undetectable with the setup shown in Fig. 2. For example, the filamentation extent for the cases shown in Fig. 3 is 315 cm for the 35 fs-long pulse, and 380 cm and 340 cm for the positively and negatively chirped pulses, respectively.

The correlation between the length of the generated plasma channels and the magnitude of the on-axis emission is evident. The energy emitted by the Bessel-Gauss beam along the axis exceeds 10% of the total input pulse energy, for the positively chirped 660 fs-long pulse. This emission is strong enough to create a plasma channel on its own. This secondary plasma channel is connected to the primary channel generated by the Bessel-Gauss beam, and the combined length of the two filaments can exceed the length of the linear focus zone of the beam.

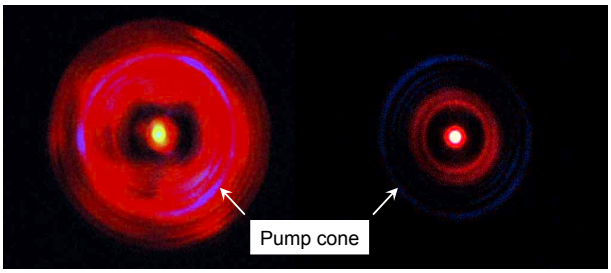

Fig. 5. Photographs of the far-field beam patterns. Only visible part of the beam spectrum is recorded. Left: Fully compressed pulse with 35 fs FWHM pulselength; Right: Positively chirped pulse with FWHM pulselength of 660 fs that maximizes the longitudinal extent of filamentation. The white spot on the beam axis that corresponds to the on-axis emission by the Bessel-Gauss beam is clearly visible in both cases. While emission into multiple cones is stronger in case of the transform-limited pulse, the on-axis emission is brighter for the chirped pulse. The faint blue ring in the pattern for the chirped pulse corresponds to the position of the main axicon ring in the far field (the pump cone).

In Fig. 5, we show photographs of the beam patterns in the far-field, for the 35 fs-long input pulse (left) and for the positively chirped 660 fs-long pulse that results in the longest generated plasma channel (right). The photographs are taken by a commercial digital camera. In this photographs, the infrared part of spectrum, including 800 nm, is blocked by a filter incorporated into the camera, and only visible part of spectrum is recorded. The nonlinear interactions in the high-intensity Bessel-Gauss beam result in the intensity re-distribution in the cross section of the beam on propagation. For the shortest pulse with high peak power density, the energy is re-distributed across the entire cross-section of the beam. For the longer pulse that generates the longest plasma channel, the energy is primarily deposited into radiation propagating close to the beam axis.

In order to quantify the radial intensity distribution in the far-field, we varied the diameter of the aperture shown in Fig. 1, and measured pulse energy propagating close to the beam axis. This data is summarized in Fig. 6. One of the curves corresponds to the case of a very long pulse (2 ps FWHM pulselength), which is assumed to propagate in a close-to-linear regime. No bright on-axis emission that is associated with filamentation was observed in this case.

#103538 - $15.00 USD Received 3 Nov 2008; revised 29 Dec 2008; accepted 3 Jan 2009; published 7 Jan 2009

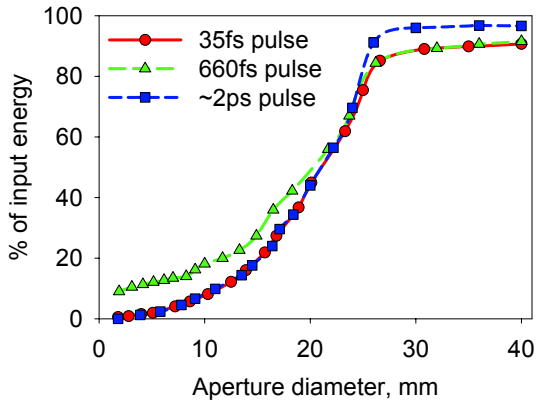

Fig. 6. Energy of the on-axis emission passing through an aperture placed 4 m away from the axicon vs. diameter of the aperture. Different curves correspond to three different durations of the laser pulse: 35 fs is the duration of the shortest pulse used in the experiments; 660 fs pulse is positively chirped, it corresponds to the longest generated plasma channel; 2 ps pulse is assumed to propagate in the close-to-linear regime. The energy emitted on axis is plotted relative to the input pulse energy.

Several conclusions can be drawn based on the data. First, the amount of energy lost by the beam into plasma generation is below 10% both for the shortest pulse and for the 660 fs-long positively chirped pulse that results in the longest filament. The overall energy loss by the 2 ps pulse is negligible, as expected. Second, in the case of the chirped pulse, the energy emitted on-axis travels in a narrow cone immediately adjacent to the beam axis. The amount of this radiation exceeds 10% of the input pulse energy, which, as the experiment shows, is sufficient for generating a plasma channel. The angular divergence of the radial component is found to be in the milliradian range. The radiation propagating close to the beam axis in the case of the shortest pulse is quite weak ($\sim$1.5% of the input pulse energy, in agreement with the data shown in Fig. 4).

4. Discussion

In what follows, we describe a qualitative argument that elucidates the role that the pulse chirp plays in the enhancement of the on-axis emission and extension of the generated plasma channel. Since the experimental observations are approximately independent of the sign of the chirp, and because the optimum pulse durations that result in generation of longest filaments are quite large, we assume that the observed effect is due more to the long pulse duration (and concomitant lower intensity) rather than it is directly related to the chirp.

In order to explain the enhancement of the on-axis emission that results from chirping the pulse, we assume that this emission is a result of a four-wave mixing (FWM) process that involves conversion of two photons from the primary Bessel-Gauss beam into idler and signal photons. It is natural to assume that the on-axis emission is maximized when both signal and idler photons are generated along the beam axis. Due to the conical nature of the Bessel-Gauss beam, we can further assume that the "incoming" pair of photons obeys the linear dispersion relation. On the other hand, both signal and idler radiation propagate in the form of transversally localized wavepackets that experience the nonlinear modification of the refractive index in the close vicinity of the beam axis.

To fulfill the phase-matching conditions for such interaction, the energy and momentum conservation have to be satisfied. Because of the strong localization of the nonlinear medium

#103538 - $15.00 USD Received 3 Nov 2008; revised 29 Dec 2008; accepted 3 Jan 2009; published 7 Jan 2009

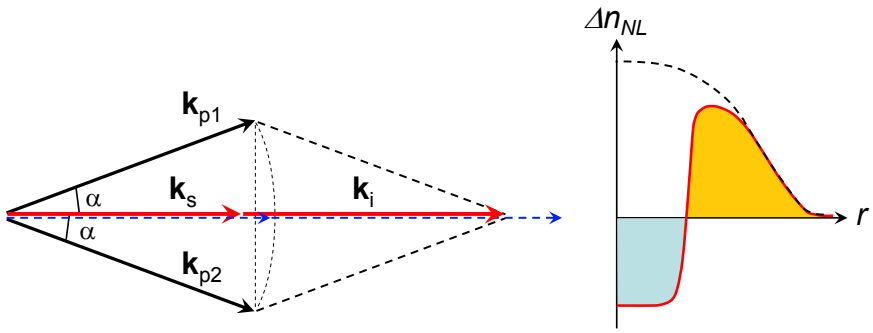

Fig. 7. Left: Momentum conservation diagram for a FWM process that involves two pump photons from the main Bessel-Gauss beam and signal and idler photons, both of which propagate along the beam axis. K-vectors for the signal and idler waves in the linear regime are shown in blue, and the wave vectors modified by the plasma contribution are shown in red. Right: Illustration of the refractive index distribution near the beam axis, in the nonlinear propagation regime. Around the axis, the index is depressed due to the generated plasma, while further from the axis the index is enhanced via Kerr effect. For long pulses, the two effects approximately balance each other so that their contributions to the effective indices for the localized signal and idler wavepackets propagating along the beam axis are of the same order of magnitude. When avalanche ionization contributes to the plasma generation, the width of the index-depressed region may become comparable to that of the region with positive contribution from the Kerr effect.

response in the on-axis region, only the longitudinal component of momentum needs to be considered explicitly. Referring to the diagram shown in Fig. 7 (left), the conservation laws read:

$$\begin{aligned} \frac{2}{\lambda_p} &= \frac{1}{\lambda_s} + \frac{1}{\lambda_i} \\ \frac{2}{\lambda_p} n_p \cos(\alpha) &= \frac{n_s}{\lambda_s} + \frac{n_i}{\lambda_i} \end{aligned} \tag{1}$$

where λ_p, λ_s, and λ_i are the vacuum wavelengths of the pump, signal and idler waves, respectively, $n_{p,s,i}$ are the effective refractive indices for the three waves, and α is the angle between the beam axis and the pump waves. For a Bessel-Gauss beam generated by an axicon lens with the tip angle θ, $\alpha \approx \theta \cdot (n_{glass} - 1)$, where n_{glass} is the refractive index of the axicon glass.

$n_{s,i}$ represent effective indices of the wavepackets that have finite overlap with the on-axis nonlinear index modification. For the purpose of our qualitative argument, we neglect the influence of chromatic dispersion on $n_{s,i}$. Then, both signal and idler waves travel along the beam axis with the same effective refractive indices. These indices are modified by the presence of the strong pump wave, so that $n_s = n_i = n_0 + \Delta n_{NL}$, where n_0 is the linear refractive index of air, and Δn_{NL} is the contribution from nonlinearity. We further assume that the pump waves travel in a close to linear regime, thus $n_p = n_0$. Using $\cos(\alpha) \approx 1 - \alpha^2/2$ and $n_0 \approx 1$, equations (1) can be rearranged to yield:

$$\Delta n_{NL} \approx -\frac{\alpha^2}{2} \tag{2}$$

As illustrated in Fig. 7 (right), the refractive index of air in the vicinity of the beam axis is modified by the positive contribution from the Kerr effect and by the negative contribution

#103538 - $15.00 USD Received 3 Nov 2008; revised 29 Dec 2008; accepted 3 Jan 2009; published 7 Jan 2009

from the generated plasma. Let us consider the two contributions in cases of short and long pulses.

For a short pulse, the Kerr effect effectively increases the on-axis propagation constant. The self-focusing collapse is arrested with the help from the generated plasma, which is mainly generated by the multiphoton ionization and only balances the beam in a dynamic sense [18]. The generated plasma lags the pulse in time and, on the average, the nonlinear index modification is dominated by the positive Kerr contribution. As a consequence, the phase-matching conditions cannot be satisfied for on-axis propagation.

For the case of a long pulse with a pulselength in the hundreds of femtoseconds range, the intensity is lower, but the avalanche ionization becomes a major player that makes plasma generation more efficient. The generated plasma overlaps with a large portion of the pulse in the time domain. The positive contribution to the nonlinear index by the Kerr effect is decreased because of the lower intensity, while the effective negative contribution due to plasma is increased due to higher overlap between the pulse and the generated plasma in time domain. If the plasma density becomes sufficiently high over a significant portion of the pulse duration, the effective index modification for the signal and idler wavepackets may become negative and the above phase-matching relation can be fulfilled.

For even longer pulses, the intensities decrease, self-focusing switches off, and eventually no filament is created. Thus, an optimal value of the duration of the chirped pulse will exist, for which the avalanche-mediated plasma generation allows the phase matching conditions to be satisfied.

Let us make some order-of-magnitude estimates in order to verify that the described scenario is indeed a plausible explanation of our experimental results. Note that it is notoriously difficult to make quantitative estimates of plasma densities generated inside filaments in terms of the medium and pulse parameters. However, we can rely on the fact that the plasma and Kerr contributions to the nonlinear index modification are opposite and tend to be of the same order of magnitude (although there is never a perfect steady-state balance between the two effects).

The Kerr contribution is essentially governed by the peak intensity in the Bessel-Gauss beam I_{peak}, that can be roughly estimated using the following formula derived for the case of axicon focusing in the linear propagation regime [19]:

$$I_{peak} = \frac{2\pi^2}{\lambda_p}\alpha w_0 \exp(-0.5)\cdot I_0 \approx 12\cdot\alpha\frac{w_0}{\lambda_p}\cdot I_0 \tag{3}$$

where w_0 is the $1/e$-amplitude radius of the Gaussian beam incident on the axicon, and I_0 is the input peak intensity of the beam, which is related to the pulse energy ε_{pulse}, FWHM pulselength T and w_0 as follows:

$$I_0 = \frac{8\sqrt{\ln(2)}}{\pi^2}\cdot\frac{\varepsilon_{pulse}}{w_0^2 T} \approx 0.67\frac{\varepsilon_{pulse}}{w_0^2 T} \tag{4}$$

Thus the Kerr contribution to the refractive index scales as

$$n_2 I_{peak} \approx 8\frac{\alpha n_2 \varepsilon_{pulse}}{\lambda w_0 T} \tag{5}$$

By the above argument, for long pulses, the overall modification of the refractive index Δn_{NL} is dominated by the plasma contribution, which is opposite in sign and of the same order of magnitude as (5). Equating the absolute values of (2) and (5) and using $\alpha \approx \theta\cdot(n_{glass}-1)$, we find the following estimate for the pulselength that satisfies the phasematching condition for the FWM process with both signal and idler waves emitted along the axis:

$$T \approx 16\frac{n_2\varepsilon_{pulse}}{(n_{glass}-1)\theta w_0\lambda_p} \tag{6}$$

#103538 - $15.00 USD Received 3 Nov 2008; revised 29 Dec 2008; accepted 3 Jan 2009; published 7 Jan 2009

In our experiment, the pulse energy is 14 mJ, $\theta = 0.38^{\circ}$, $w_0 = 5$mm, and $\lambda_p \approx 0.8\mu$m. The nonlinear index of air $n_2 \approx 3.2 \cdot 10^{-23}$ m^2/W, and $n_{glass} = 1.45$. Using these parameters in the formula (6) above, we estimate the pulselength that fulfills the phasematching conditions in our experiment at 605 fs. For the simple model used and the number and degree of approximations made, this result agrees remarkably well with the experimentally found values of 660 fs and 615 fs for the positively and negatively chirped pulses, respectively.

We point out that the above formula (6) cannot by any means be considered a rigorous result. The drawback of our argument is that the magnitude of the effective index modification due to the Kerr and plasma effects cannot be evaluated without knowing the actual shape of the on-axis propagating wavepackets. Yet, the agreement between the order of magnitude estimation above with the experimental results suggests that the proposed scenario is feasible.

5. Conclusion

In conclusion, we experimentally studied extended filamentation with temporally chirped femtosecond Bessel-Gauss beams in air. We found that the longitudinal extent of the plasma channels is maximized for a particular duration of the chirped pulses. The effect was found to be related to the emission of a strong on-axis component along the beam axis that, under certain conditions, attains sufficient energy to initiate filamentation on its own. We attributed the on-axis emission by the femtosecond Bessel-Gauss beam to the nonlinear four-wave mixing process in which both signal and idler waves are emitted along the beam axis. Using plasma-assisted phasematching considerations, we derived a simple formula that relates the pulselength of the chirped pulse that results in longest filament, to the relevant experimental parameters. Estimates based on this formula are found to be in good agreement with the experiments.

Acknowledgments

This work was supported by the US Air Force Office of Scientific Research (AFOSR) under contracts FA9550-07-1-0010 and FA9550-07-1-0256.

#103538 - $15.00 USD Received 3 Nov 2008; revised 29 Dec 2008; accepted 3 Jan 2009; published 7 Jan 2009